A bronchoscopic microwave ablation applicator: Theoretical and experimental investigation

by

Austin Pfannenstiel

B.S., Kansas State University, 2009
MBA, Kansas State University, 2017

A THESIS

submitted in partial fulfillment of the requirements for the degree

MASTER OF SCIENCE

Department of Electrical and Computer Engineering
College of Engineering

KANSAS STATE UNIVERSITY
Manhattan, Kansas

2018

Approved by:

Major Professor
Dr. Punit Prakash

Copyright

Abstract

Microwave ablation (MWA) is a minimally invasive thermal therapy predominantly used in the treatment of localized cancer. Previous studies have demonstrated clinical use of MWA for treating lung tumors, however, these procedures have relied upon the use of rigid percutaneous MWA applicators which can limit the range of accessible tumors and may have inherent disadvantages for use in lung tissue. The objective of this work was to develop and characterize a bronchoscopic MWA applicator suitable for use in a system that enables bronchoscopic transparencymal nodule access (BTPNA). A 3D coupled FEM electromagnetic-heat transfer model was implemented to optimize the antenna design and evaluate the expected ablation size and shape. A prototype device was fabricated and experimentally evaluated in *ex vivo* tissue to verify simulation results and demonstrate proof-of-concept. Simulated and experimental results indicate the proposed device could create ablation zones 19.3 – 31.0 mm in diameter with 30 – 45 W of power applied for 5 – 10 minutes. Future bronchoscopic MWA applicators based on the design proposed in this study could allow physicians an even less invasive treatment option for lung cancer with increased accuracy and efficacy and reduced risk of procedural complications immediately following a positive bronchoscopic lung biopsy.

Table of Contents

List of Figures

List of Tables

Acknowledgements

I would like to acknowledge several students and colleagues who have helped me produce the work described in this thesis. All the students and faculty of Kansas State University's Biomedical Computing and Devices Lab have been fantastic assets, but I would like to specially thank Jan Sebek for helping introduce me to COMSOL and Hojjat Fallahi for sharing his dielectric property measurements of water and various *ex vivo* tissues.

I would also like to acknowledge my industry collaborators at Broncus Medical, Henkey Wibowo, Tom Keast, and Steve Kramer, for providing funding and guidance and for sharing their industry experience.

Finally, I would like to thank my committee members Dr. William Kuhn, Dr. Jungkwun Kim, and Dr. Punit Prakash for helping me review and improve this thesis. I would like to especially thank Dr. Prakash for sharing so much of his time, mentorship, and experience with me over the last couple of years.

Dedication

I would like to first dedicate this thesis to my parents, Mitch and Robin. They have shown me the importance of hard work and instilled in me a confidence that I can accomplish anything.

I would also like to dedicate this thesis to my loving wife, Sarah. She takes wonderful care of me and is the perfect partner.

Chapter 1 - Background

I. Introduction

Thermal therapy is a growing medical field which utilizes a wide range of biomedical devices and systems to heat tissue for direct or indirect treatment of disease. Some thermal therapy systems are designed to moderately heat tissue (~41 - 43 °C) for a sustained duration (~30 – 60 minutes) with the typical goal of increasing blood flow to the region and locally enhancing the effects of drug delivery or ionizing radiation treatment [1]. Other thermal therapy processes, commonly referred to as thermal ablation, aim to directly destroy disease by raising tissue temperatures above which irreversible damage occurs. Cell death by thermal ablation is probabilistic and depends both on maximum temperature achieved and the time exposed to elevated temperatures [2]. However, at temperatures near 55 – 60 °C, cell death is almost instantaneous [3]. Several different energy modalities have been utilized for thermal therapy including high-intensity focused ultrasound, laser, thermal conduction, radiofrequency, and microwave in a range of non-invasive or minimally invasive systems [4]–[8]. There are also numerous non-oncological applications of thermal therapy such as treatment of cardiac arrhythmia, benign prostate hyperplasia, or chronic nerve pain [9]–[11].

Microwave ablation (MWA) is a type of minimally invasive thermal therapy predominantly used in the treatment of localized cancer. During microwave ablation, the cellular damage results from kinetic heating of polar molecules (such as water and proteins) that rapidly oscillate as they try to align with the applied electromagnetic waves. The goal of MWA is to heat a target area surrounding a tumor to toxic temperatures while minimizing damage to surrounding healthy tissues and the probability of medical complications. The target ablation zone typically includes a 5 – 10 mm margin on all sides of the tumor to ensure complete destruction of the known diseased tissue as well as any microscopic disease surrounding the tumor that may be undetected on diagnostic imaging (see Figure 1-1).

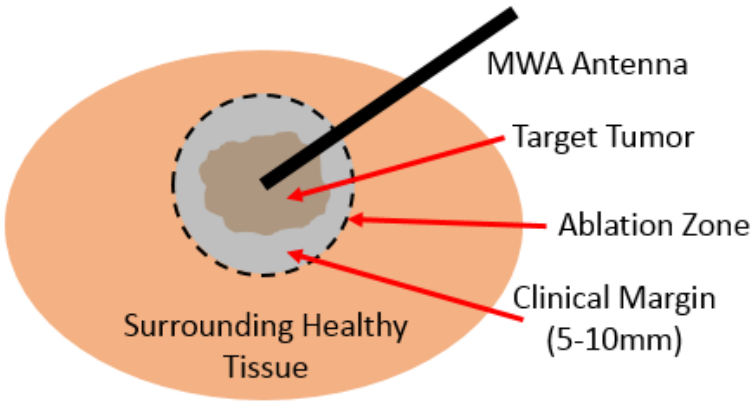

Figure 1-1 Thermal Ablation Zone with Clinical Margin

The rate of heating as well as the penetration depth of microwave energy is dependent on the specific target tissue's dielectric properties (which are highly dependent on the tissue's water/blood content). In general, biological materials could be classified as lossy dielectrics with typical effective conductivities ranging from 1 – 2 [S/m] and relative permittivities ranging from 20-60. Tissues with a higher conductivity absorb a greater fraction of the applied electromagnetic (EM) field, resulting in a higher heating rate and reduced penetration depth. Tissues with a higher relative permittivity result in a shorter wavelength for a given applied EM frequency which allow for smaller overall MWA antenna dimensions, creating a less invasive applicator. A list of common MWA target tissue types as well as their applicable properties is given in Table 1-1. Other factors affecting the heating rate and overall ablation size and shape include a tissue's thermal conductivity and the heat sink effect due to blood perfusion and proximity to blood vessels or arteries. Currently available systems operate at 915 MHz or 2.45 GHz, both of which lie within frequency bands approved for industrial scientific and medical (ISM) use, though higher frequency systems are being investigated in research studies [12], [13]. MWA antennas operating at 915 MHz and 2.45 GHz have been compared by Curto et al. where simulated and experimental results showed antennas operating at 2.45 GHz produced both larger and more spherical ablation zones [14]. However, higher frequency 2.45 GHz systems do result in increased attenuation, power loss, and waste heat generation within applicators compared to systems operating at 915 MHz. These effects can typically be compensated for with higher input powers and forced cooling systems.

Table 1-1 Typical MWA Target Tissue Electrical Properties

Target tissue	*Relative Permittivity* ε_r	*Effective Conductivity* σ *[S/m]*	*Wavelength* λ *[m]*	*Penetration Depth [m]*
Liver – 915 MHz [15]	46.76	0.86	0.047	0.042
Liver – 2.45 GHz [15]	43.04	1.67	0.018	0.021
Deflated Lung – 915 MHz [15]	51.37	0.86	0.45	0.044
Deflated Lung – 2.45 GHz [15]	48.31	1.68	0.017	0.022
Inflated Lung – 915 MHz [15]	21.97	0.46	0.069	0.055
Inflated Lung – 2.45 GHz [15]	20.48	0.80	0.027	0.030
Kidney – 915 MHz [15]	58.56	1.40	0.042	0.029
Kidney – 2.45 GHz [15]	52.74	2.43	0.017	0.016
Brain – 915 MHz [15]	38.84	0.60	0.052	0.056
Brain – 2.45 GHz [15]	36.17	1.21	0.020	0.026

The objectives of MWA antenna design are twofold. First is maximizing power transfer to the target. This is accomplished by carefully matching the antenna's impedance (which is determined by the antenna dimensions and electrical properties of materials surrounding the applicator, i.e., the combination of tumor, healthy tissue, cooling water, insulating catheter, etc.) to that of the feeding transmission line. A well-matched antenna will enable the transfer of a large fraction of the incident power to the tissue with less power being reflected back to the source, allowing for shorter treatment times, lower applied powers, and less unwanted heating of the applicator or system cabling from attenuation (which may also alter the shape of the thermal ablation zone). A common way to evaluate antenna power transfer is through measuring the antenna's reflection coefficient at the input port, S_{11}:

$$S_{11} = \frac{V_1^-}{V_1^+} = \frac{Refelcted\ Voltage\ Wave}{Incident\ Voltage\ Wave}$$

In practice, antenna designs with a S_{11} of at -10 dB or better (more negative) are desired for MWA applicators so 90% or more of the incident power is transferred to the target.

The second goal in MWA antenna design is to achieve a large, spherical ablation zone. Larger ablation zones enable the treatment of larger tumors while still maintaining the desired clinical margin. More spherical ablation zones are desired for treatment planning since physicians can intuitively map spheres to target single small/medium tumors or overlap multiple spheres to target large tumors [16]. Also, many tumors generally have a spherical shape and therefore spherical ablation zones help spare more healthy surrounding tissue and avoid damage to nearby critical structures. Ideally, a MWA applicator could produce nearly spherical ablation zones with nearly constant dimensional ratios as applied power/time is scaled to treat tumors of various diameters. A MWA applicator's ablation zone can be shaped by changing the type of antenna (i.e. monopole, dipole, slot, helix, etc.) or modifying and shaping the materials which make up the remainder of the MWA applicator (i.e. insulating catheter materials or presence of cooling water or another medium surrounding the antenna).

A first order method to evaluate the shape of an antenna's expected thermal ablation zone is through analysis of its electromagnetic specific absorption rate (SAR) profile in the target tissue. The SAR profile only gives the rate at which EM energy is absorbed in the surrounding medium, and does not account for other thermal effects such as heat conduction, water vaporization in the surrounding tissue, or heat losses to blood perfusion, but has been shown to be an effective measure for optimizing ablation zone shape [17]. The normalized SAR profiles for simplified insulated monopole and dipole MWA antenna designs are shown in Figure 1-2 below (which are very similar for a basic design). In some cases, MWA antennas may include a balun or choke to reduce outer surface currents and improve on the typical SAR teardrop shape, however, in general these add complexity to the design and increase the overall device diameter [18], [19]. Another method to compensate for the SAR tail or teardrop shape (see Figure 1-2) to produce more spherical thermal ablation zones is forced cooling of the applicator shaft.

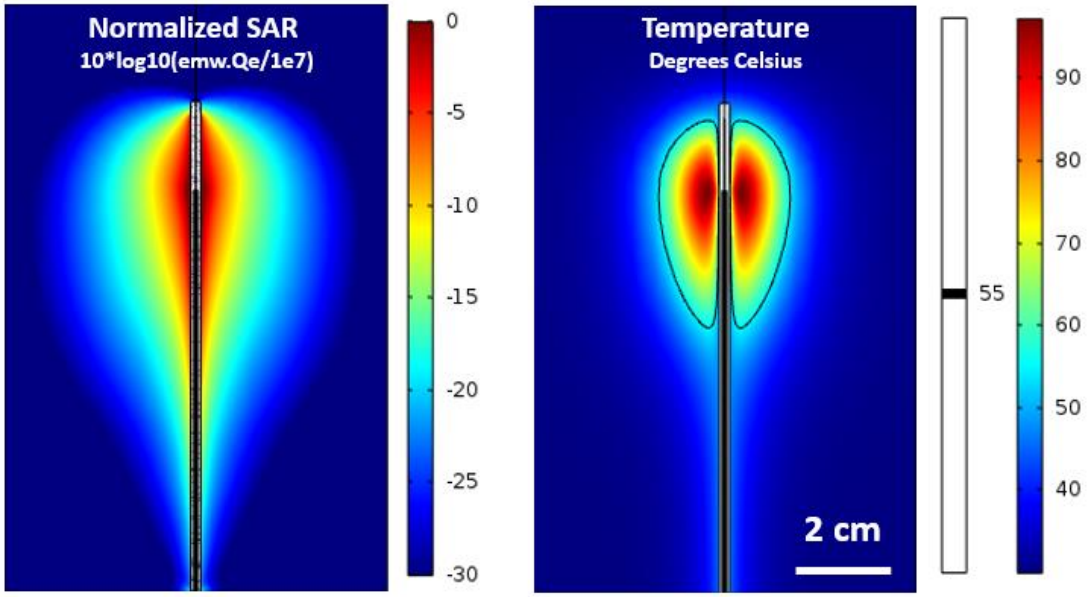

Figure 1-2 Normalized Specific Absorption Rate (SAR) and Temperature Patterns for Insulated Monopole Antenna

There are currently seven FDA approved MWA systems in the USA, however, clinical application is limited to percutaneous treatment of unresectable tumors in the liver, lung, and kidney [12]. MWA systems are also under development for non-oncologic applications such as treatment of prostate hyperplasia and cardiac arrhythmia [10], [20]. A block diagram for a typical MWA system is given in Figure 1-3. Current systems are heavily reliant on individual physician skill and experience to provide effective treatment because of several technical challenges. Although efforts have been made to integrate diagnostic imaging with overlays of predicted ablation zones, treatment planning still mostly consists of physicians using their experience to scale manufacturer supplied charts of ablation size vs power/time in *ex vivo* bovine liver tissue when treating a range of tumor types in human patients. Second, image guidance is typically used for initial tumor diagnosis, during the procedure to guide applicator placement, and post-procedure to confirm the size of the ablation zone; however, there are no practical ways to use imaging to monitor growth of the thermal ablation zone in real time. Measuring temperature changes with MRI is possible, but is very expensive and is technically challenging to integrate with MWA applicators and systems [21]. Intra-procedural feedback systems, which could theoretically take real-time data from imaging or antenna performance to monitor ablation progress, have been proposed in literature, but have yet to be implemented clinically.

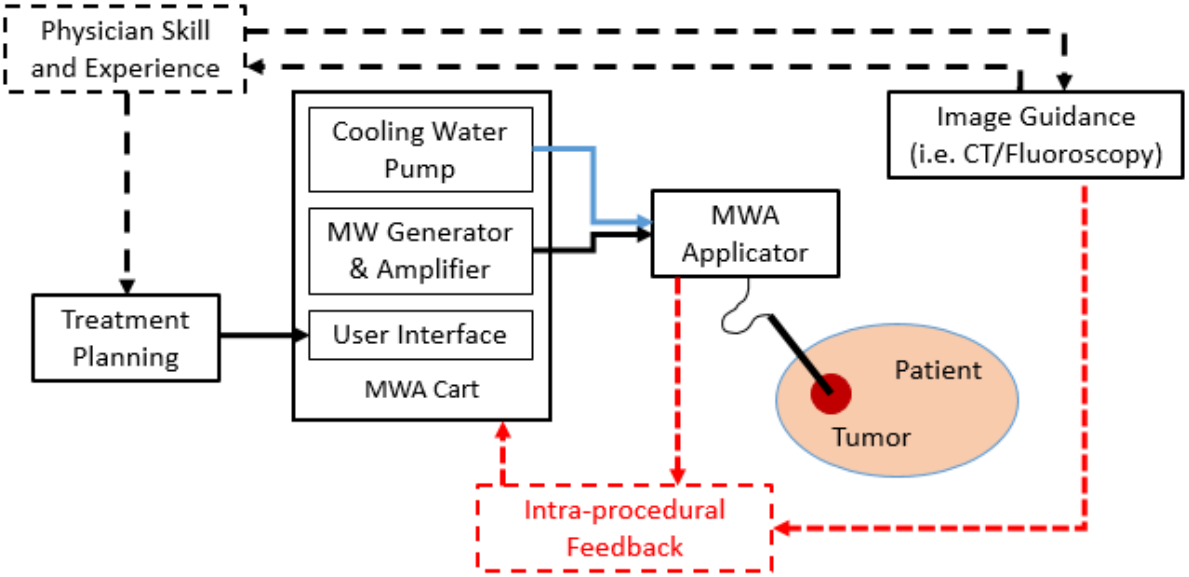

Figure 1-3 Block Diagram of MWA System

Despite current limitations, MWA has major advantages over traditional surgical resection including a less invasive, less time consuming procedure with shorter patient recovery times and lower complication rates [12]. Additionally, MWA may offer a treatment option for some high-risk patients who would otherwise be ineligible for surgical resection or other physically demanding therapies due to medical complications. MWA also has several advantages over other thermal ablation energy modalities such as radiofrequency ablation (RFA) or cryoablation. These include the potential to produce faster heating over larger volumes, less impact from heat sinks such as blood vessels, effectiveness in high impedance aerated (lung) or desiccated tissues, the ability to utilize multiple applicators to produce larger ablation zones, and fewer ancillary components (such as grounding pads). Ultimately, these advantages should help produce more uniform ablations with shorter treatment times [22], [23]. A disadvantage is increased attenuation in connecting cables causing reduced power delivery and creating waste heat that may need to be compensated for by active cooling mechanisms.

However, the use of rigid MWA applicators, which must be inserted percutaneously, restricts the ability to treat patients with a variety of challenging tumor sizes, shapes, and locations. Some lesions, such as centrally located lung tumors, simply cannot be accessed via this approach. Other times, surrounding structures such as bones, major arteries, or nerves limit the application of percutaneous devices. Furthermore, physicians must currently rely only on their intuitive ability

to interpret 2-D imaging, such as fluoroscopy or ultrasound, when attempting to accurately place a percutaneous MWA device in a 3-D environment during a procedure. A misplaced applicator has shown to have a significant effect on the overall treatment margin [24]. As a consequence, the patient's outcome is highly dependent on the clinical accessibility of their tumor and an individual physician's skill and experience. An illustration of some of the potential challenges to safe and effective MWA are show in Figure 1-4. For lung tumors, ablation near critical structures could result in damage to the esophagus, major vessels and arteries, or the heart causing pain or potentially life-threatening complications [25], [26]. Ablation in close proximity to the pleural surface near the chest wall could cause pneumothorax. Pneumothorax occurs when air leaks into the space between the lung and chest wall and can collapse the lung. Most cases occurring during lung MWA are minor, but more severe cases require hospitalization and chest tube placement [12], [23]. Incomplete ablation or inaccurate applicator placement could result in disease recurrence [27], [28].

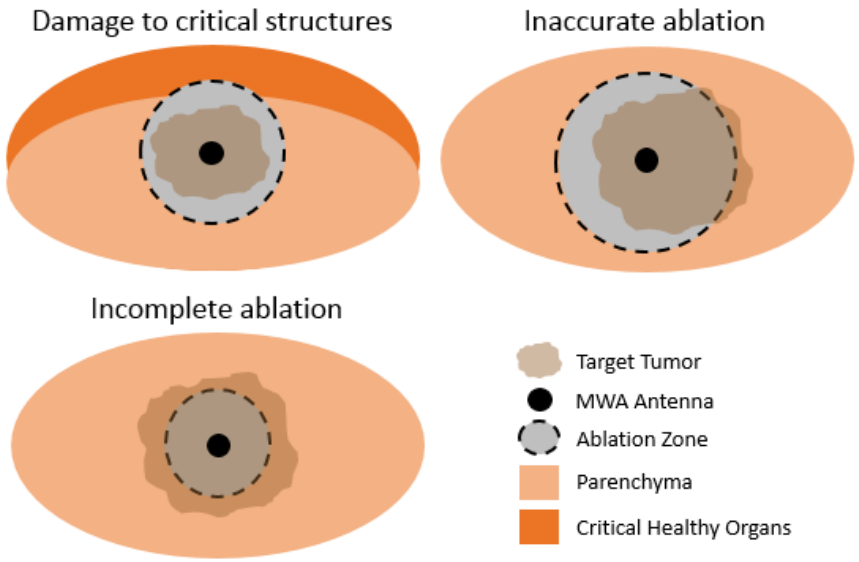

Figure 1-4 MWA Challenges

Improving the capabilities and effectiveness of MWA procedures may not only lead to better treatment outcomes for patients who have run out of other options, but could also encourage its use for many thousands more currently facing high risk surgeries or debilitating side effects from chemotherapy drugs and radiation.

II. The Rationale for a Bronchoscopic MWA Approach

According to the American Cancer Society, lung cancer is the second most common type of cancer for both men and women and accounts for 14% of all new cancers [29]. An estimated 234,030 new cases of lung cancer will be diagnosed with an estimated 154,050 death from lung cancer in 2018 [29]. Furthermore, lung cancer is the leading cause of cancer deaths in both men and women, accounting for 1 in 4 cancer deaths in the Unites States [29]. This is especially troubling because only a small minority (about 30%) of those diagnosed are potential candidates for traditional surgery [12].

Historically, lung cancer has been difficult to diagnose at an early stage, which is a major contributor to its mortality [30]. In fact, many small pulmonary nodules (< 3 cm) are identified accidentally from chest radiographs or computed tomography (CT) scans that are taken for other purposes [30]. However, the continued improvement and increased use of CT scanning has increased the identification rates of small lesions and CT has been demonstrated to be an effective lung cancer screening tool [31]. Once a lung a lesion is identified, a physician still faces several choices including continued radiographic observation, metabolic PET imaging, biopsy, or immediate surgical resection [32]. The gold standard for lung cancer diagnosis is to collect a sample of tissue from the lesion with a biopsy and analyze it pathologically [31].

To perform a biopsy, a physician traditionally had two preferred options: transthoracic needle aspiration (TTNA) or transbronchial biopsy using a bronchoscope [33]. TTNA has a high diagnostic yield (90%), but has a high rate of complications with 15-35% resulting in pneumothorax and 6% requiring chest tube placement [31], [33]. Alternatively, the overall rate of complications for bronchoscopy is much lower (< 2%), but the diagnostic yield is also lower (13-60%) [33]. To combine the advantages of both methods, a new biopsy technique, bronchoscopic transparenchymal module access (BTPNA), has been developed that can create a direct pathway from the bronchus to the target without relying on the anatomy of the airways [32], [33]. In pilot studies BTPNA diagnostic yield was 90.3% with no significant complications in any canine subjects [32].

Similar to TTNA, percutaneous MWA of lung malignancies is effective, but also associated with a comparatively high risk of complications such as pneumothorax with an occurrence rate of 39% and 43% reported in two studies [23], [27]. Furthermore, the risk of severe pneumothorax may be exacerbated by tissue contraction known to occur during MWA for lesions

located near the pleural surface [34]. Wolf et al. noted pleural retraction and dimpling in several post ablation resection specimens [27]. Piggybacking on the development of BTPNA procedures, a novel, long, flexible, bronchoscopic MWA applicator may also be able to span the best of both worlds by providing an effective treatment while minimizing invasiveness and the risk of complications. Furthermore, rather than subjecting a patient to multiple hospital visits, a bronchoscopic MWA applicator could facilitate immediate treatment of malignancies identified during BTPNA. Finally, bronchoscopic MWA may enable treatment of central lesions which are difficult to access percutaneously due to obstructions such as bones, blood vessels, or other critical structures.

To take advantage of the increased access afforded by a bronchoscopic MWA applicator, a robust visualization and navigation platform is necessary to accurately reach target tumors. Our industry partner, Broncus Medical, has developed the Archimedes™ system which integrates virtual bronchoscopic navigation with optimized BTPNA tunnel planning and guidance [35], [36]. The goal of the work described in the next chapter is to develop a bronchoscopic MWA applicator that could be used to expand the functionality of the Archimedes system to include disease treatment. Figure 1-5 shows a bronchoscopic MWA approach vs a percutaneous approach.

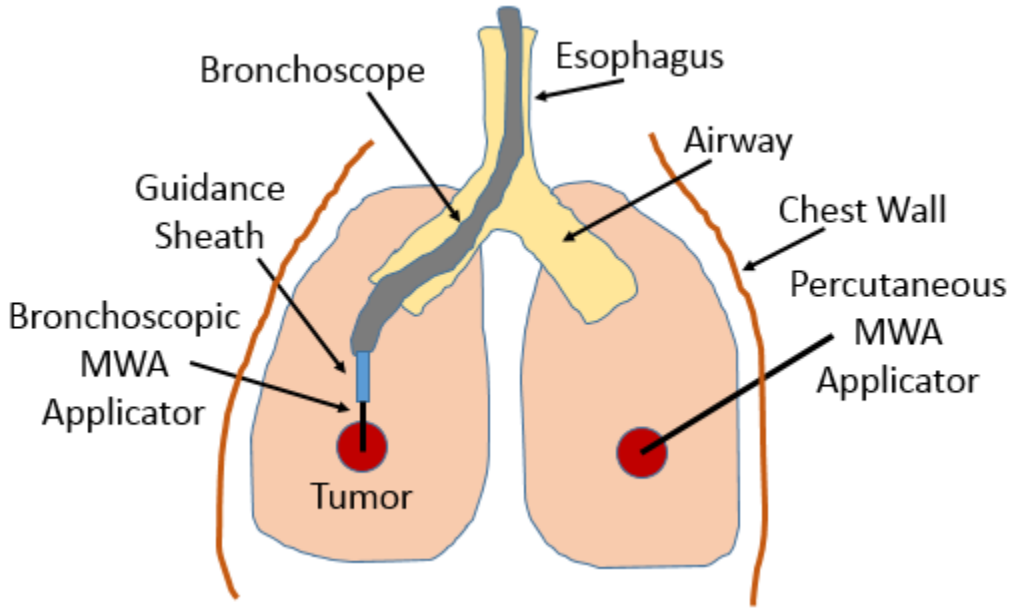

Figure 1-5 Bronchoscopic Approach vs Percutaneous Approach

III. Bronchoscopic MWA Applicator Design and Performance Goals

A bronchoscopic MWA applicator is significantly different from percutaneous MWA applicators already in clinical use several key ways. First, it must be very long, up to 1.5 m long, so it can be threaded through the operating channel of bronchoscope and still reach targets located in peripheral areas of the lung. This compares to the 15-30 cm length of typical percutaneous applicators and contributes several engineering challenges such as increased power loss and heat generation from attenuation. Second, it must be flexible, able to negotiate a tight bend radius if the bronchoscopic must be fully articulated to reach the target site. Nearly all other MWA applicators in clinical use are rigid, needle-like designs intended to be inserted in the target percutaneously under image guidance. Finally, a bronchoscopic MWA applicator must have a very small outside diameter, less than 1.9 mm, to fit inside a bronchoscope's working channel. Although current percutaneous MWA applicators all strive for the smallest achievable outside diameter to minimize procedure invasiveness, it is not a design constraint. Some current MWA applicators are a small as 17 gauge (1.47 mm OD), while others can be as large at 14 gauge (2.108 mm OD) [37], [38]. Figure 1-6 shows a prototype bronchoscopic MWA applicator compared to a percutaneous applicator and inserted in the working channel of a bronchoscope.

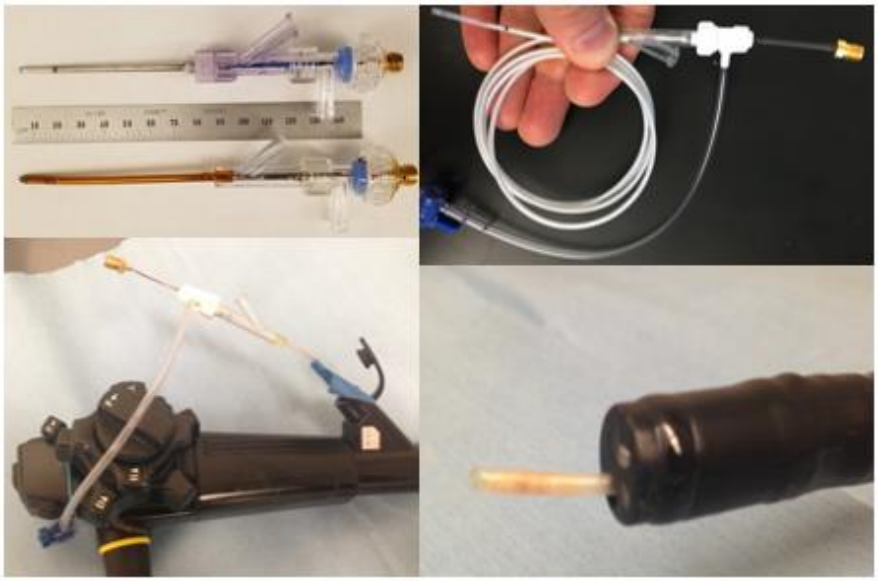

Figure 1-6 Prototype Bronchoscopic MWA Applicator Compared to Percutaneous Applicator; Bronchoscopic Applicator Inserted in Bronchoscope Working Channel

The principle use for a bronchoscopic MWA applicator would be the treatment of the growing number of small lung nodules being identified by improved resolution chest CT scans. Previously, these nodules would have been left untreated and monitored until they grow to a size requiring surgical resection, radiation therapy, or a systemic treatment such as chemotherapy. These tumors could instead be treated immediately (during the same procedure) once identified as malignant during as a bronchoscopic biopsy. The expectation is most of these tumors would be relatively small, on the order of approximately 1 cm in diameter. Adding a circumferential margin of 5 mm results in a target ablation zone diameter of 2 cm. Furthermore, a very spherical ablation zone is desired to contain as much thermal damage as possible to the tumor while sparing the most healthy surrounding parenchyma. Finally, to avoid tract ablation and damage to the working channel of the bronchoscopic the surface temperature of a bronchoscopic applicator must remain below 50° C along the entire length exclusive of the active distal section.

A. Transmission Line Selection

A primary design constraint was selection of a suitable coaxial microwave transmission cable. Not only must the cable fit within the maximum outside diameter of the device, it must also deliver enough power to the MW antenna to produce the minimum required ablation zone and be flexible enough to traverse the require bend radius. Unfortunately, very thin coaxial microwave transmission cables are only rated to deliver very low power (< 10 W) and have several dB of attenuation per meter. Past experience in our group has shown it is possible to operate coaxial microwave transmission well above their rated powers with forced flow water cooling. Therefore, the bronchoscopic MWA applicator necessitated water cooling to deliver enough power to ablate (30 – 60 W) and remove the waste heat from cable attenuation while maintaining an acceptable device on contact temperature.

To provide sufficient cross-sectional area for cooling water inflow and outflow within the maximum device diameter, a UT-034 semi-rigid coaxial cable was initially selected (Microstock Inc., West Point, PA). This cable had an outside diameter of 0.034" (0.864 mm), a rated power of about 8 W, and an insertion loss of 2.9 dB/m (based on linear interpolation from the manufacturer's data sheet) at 2.45 GHz. Although named "semi-rigid," this cable was still very pliable and could also meet the required bend radius. Several prototype devices were built with this cable selection.

Unfortunately, once forced through a bend, the semi-rigid nature of UT-034 resulted in the cable, and microwave applicator, retaining a curvature. When used clinically, this would result in the applicator advancing in an unpredictable (or very difficult to predict) direction when exiting a bronchoscope that was articulated in potentially many different ways to reach the target site. This phenomenon of retaining a curvature is referred to as "set." The consequence could be the applicator not missing the target site and causing either under-ablation of the tumor or unintended damage to nearby healthy structures.

To reduce the applicator's set, a more flexible replacement transmission cable was necessary. Instead of standard semi-rigid cables, which tend to hold their shape once external forces are removed, several cables with braided center and outer conductors were evaluated. The engineering tradeoff in using a more flexible braided coaxial cable is a generally larger diameter and higher insertion loss. However, a low loss 1.13 mm diameter coaxial cable (D113LWS5BT, Wellshow, Keelung City, Taiwan) was identified with a 2.4 GHz insertion loss of 2.5 dB/m. This cable had a 2-layer outer shield consisting of Cu-PET tape and a braided tinned copper wire to minimize loss. This cable also has an outer insulating FEP outer jacket that was found to improve cooling water flow rate and reduce applicator set compared to un-jacketed braided cables. The length of outer jacket stripped from the outer conductor near the antenna was found to have an impact on antenna performance and will be discussed in more detail in the next chapter.

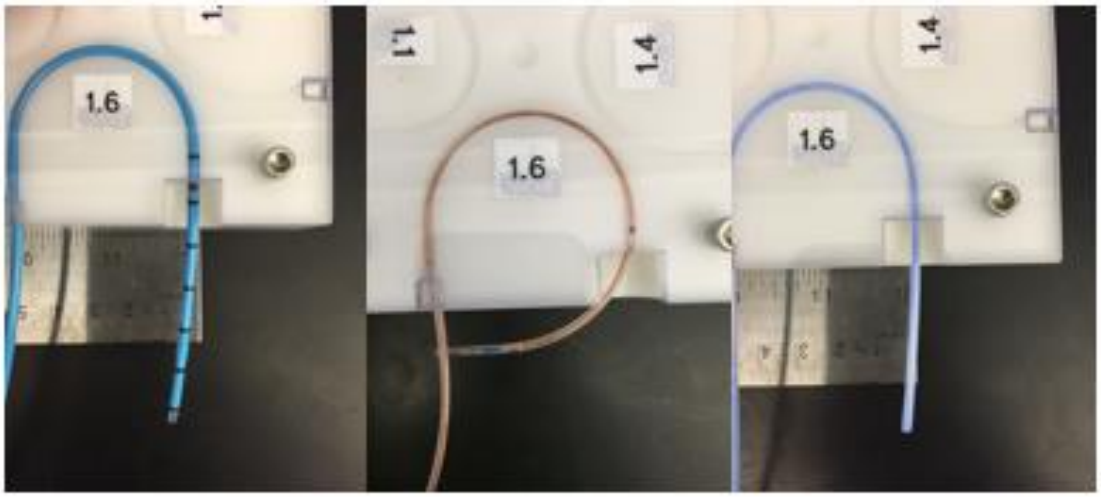

Figure 1-7 Applicator "Set" for Plastic Stylet in Sheath (left), Semi-Rigid Coax MWA Applicator (center), and Braided Coax MWA Applicator (right)

B. Outer Catheter Selection

Primary design considerations for a bronchoscopic MWA applicator outer catheter included: providing a low friction outer surface for ease of insertion through the bronchoscope operating channel, providing supply and return paths for cooling water, flexibility, and mechanical strength/durability. An original design opted for telescoped, concentric extrusions of thin-walled, PTFE tubing surrounding the UT-034 transmission cable to form the outer applicator structure and supply/return flow paths. Commercially available standard size extrusions were obtained from Zeus Inc. which met the maximum applicator OD constraint and approximately balanced the available inflow and outflow cross sectional areas.

This design was found to provide approximately 13 mL/min of flow with a peristaltic pump set at a speed a low speed (to prevent excessive internal pressures from damaging the applicator). However, applicator surface temperature was later found to be in excess of 60° C in experiments with prototypes of this design.

Due to the limited flow area caused by including an extra concentric tube inside the device, as well as the necessity to switch to the larger 1.13 mm braided cable from the UT-034 cable, a new outer catheter design was required. If instead of a telescoped, concentric tube design, a custom dual lumen extrusion with a single divider slightly offset from the central axis was used, then the total flow area could be increased by over 75% (assuming the same outer tubing and coaxial cable dimensions). The significant gains are achieved by replacing the cross-sectional area required by the inner tube (with a wall thickness of 0.15 mm) with a single rectangular divider wall (also with an assumed thickness of 0.15 mm). The offset divider would allow for a larger braided cable and inflow path to be contained in the larger lumen with the outflow path provided in the smaller lumen. Using the largest possible outer diameter, thinnest extrudable wall dimensions, and then equalizing inflow and outflow areas fixed many more of the physical dimension for the final applicator design.

IV. Lung Tumor Characteristics

The physical and electric properties of lung tumors, especially at higher frequencies and elevated temperatures, are not well reported in the literature. Lung tumor properties are anticipated to be highly variable and dependent on the specific tumor's biology (i.e. primary cancer vs.

metastatic disease) and physical characteristics (i.e. sold vs. semi-solid). Furthermore, even healthy lung has highly variable electrical properties with inflated lung having approximately half the relative permittivity of deflated lung.

Nevertheless, percutaneous MWA applicators are currently being used to treat lung tumors [12], [23], [27]. These devices were likely optimized for use in treating liver cancer with manufacturer supplied time and power dependent expected ablation zone charts provided for clinical use based on ex vivo liver characterization. Since most MWA clinical and regulatory approval experience is based on initial work in liver tissue, with individual physicians later cross-applying their experience to treat other tissues, using the more well-documented tissue properties of liver is still considered an acceptable starting point for device design.

Chapter 2 - Theoretical and Experimental Investigation

I. Introduction

According to the American Cancer Society, lung cancer is the second most common type of cancer for both men and women and accounts for 14% of all new cancers [29]. An estimated 234,030 new cases of lung cancer will be diagnosed with an estimated 154,050 deaths from lung cancer in 2018 [29]. Furthermore, lung cancer is the leading cause of cancer deaths in both men and women, accounting for 1 in 4 cancer deaths in the United States [29]. This is especially troubling because only a small minority (about 30%) of those diagnosed are potential candidates for traditional surgery, which is the gold standard treatment for lung cancer [12].

Historically, lung cancer has been difficult to diagnose at an early stage, which is a major contributor to its mortality [30]. In fact, many small pulmonary nodules (< 3 cm) are identified accidentally from chest radiographs or computed tomography (CT) scans that are taken for other purposes [30]. However, the continued improvement and increased use of CT scanning has increased the identification rates of small lesions and CT has been demonstrated to be an effective lung cancer screening tool [31]. Once a lung a lesion is identified, a physician still faces several choices including continued radiographic observation, metabolic PET imaging, biopsy, or immediate surgical resection [32]. The gold standard for lung cancer diagnosis is to collect a sample of tissue from the lesion with a biopsy and analyze it pathologically [31].

To perform a biopsy, a physician traditionally had two preferred options, transthoracic needle aspiration (TTNA) or transbronchial biopsy using a bronchoscope [33]. TTNA has a high diagnostic yield (90%), but has a high rate of complications with 15-35% of procedures resulting in pneumothorax and 6% requiring chest tube placement [31], [33]. Alternatively, the overall rate of complications for bronchoscopic biopsy is much lower (< 2%), but the diagnostic yield is also lower (13-60%) [33]. To combine the advantages of both methods a new biopsy technique, bronchoscopic transparenchymal module access (BTPNA), has been developed which can create a direct pathway from the bronchus to the target without relying on the anatomy of the airways [32], [33]. In pilot studies BTPNA diagnostic yield was 90.3% with no significant complications in any canine subjects [32].

Microwave ablation (MWA) is a minimally invasive thermal therapy that can be used to treat small to medium sized tumors. The goal of thermal ablation is heating of the target tissue to

toxic temperatures (T > ~55 °C), leading to cell death by coagulative necrosis. During microwave ablation, the mechanism of cellular damage develops from the kinetic heating of polar molecules (such as water and proteins) that rapidly oscillate as they try to align with the applied electromagnetic waves. Major advantages over traditional surgical resection include a less invasive, less time consuming procedure with shorter patient recovery times and lower complication rates [12]. Additionally, MWA may offer a treatment option for some high-risk patients who would otherwise be ineligible for surgical resection or other physically demanding therapies due to medical complications.

However, the use of rigid MWA applicators, which must be inserted percutaneously, restricts the ability to treat patients with a variety of challenging tumor sizes, shapes, and locations. Some lesions, such as centrally located lung tumors, simply cannot be accessed via this approach. Other times, surrounding structures such as bones, major arteries, or nerves limit the application of percutaneous devices. Furthermore, physicians must currently rely on their intuitive ability to interpret 2-D images from sources such as fluoroscopy or computed tomography (CT) when attempting to accurately place a percutaneous MWA device in a 3-D environment during a procedure. A misplaced applicator has been shown to have a significant effect on the overall treatment margin [24]. Consequently, the treatment outcome may be highly dependent on the clinical accessibility of the tumor and an individual physician's skill and experience.

Similar to TTNA, percutaneous MWA of lung malignancies is effective, but also associated with a comparatively high risk of complications such as pneumothorax with an occurrence rate of 39% and 43% reported in two studies [23], [27]. Furthermore, the risk of severe pneumothorax may be exacerbated by tissue contraction known to occur during MWA, especially for lesions located near the pleural surface [34]. Wolf et al. noted pleural retraction and dimpling in several post ablation resection specimens [27].

This study presents a novel, long, flexible, bronchoscopic MWA applicator that may be able to build upon new BTPNA techniques and provide an effective thermal treatment of pulmonary tumors while minimizing invasiveness and the risk of complications. The applicator consists of a coaxial transmission cable and antenna situated inside a long, flexible outer catheter that also provides a flow path for circulating cooling water. Section II details the simulation techniques employed to optimize the antenna design. Simulation and experimental results are

provided in Section III. The performance of the antenna is further discussed in Section IV and a conclusion is provided in Section V.

II. Materials and Methods

A simulation-based approach was used to optimize the design of the bronchoscopic microwave applicator. The two performance criteria evaluated during the design phase were (1) proper antenna impedance matching ensuring efficient transfer of energy from the ablation antenna to the target tissue and (2) a spherical ablation zone as measured by an axial ratio close to 1.0 (ablation width divided by the length). After optimizing antenna physical dimensions through simulation, proof-of-concept antennas were fabricated and experimentally assessed in *ex vivo* bovine liver to evaluate impedance matching and ablation zone size, validate the simulation model, and compare to current clinically available percutaneous MWA applicators. Simulations were then employed to estimate ablation performance in lung tissue *in vivo*.

A. Design Constraints and Performance Goals

A bronchoscopic MWA applicator is significantly different from percutaneous MWA applicators already in clinical use. First, it must be up to 1.5 m long, so it can be threaded through the operating channel of the bronchoscope and still reach targets located in peripheral areas of the lung. This compares to the 15-30 cm length of typical percutaneous applicators and contributes to increased power loss and waste heat generation due to attenuation in the transmission cable at microwave frequencies. For example, a 30 cm long MWA applicator made from UT-034 semi-rigid coaxial cable would have a total attenuation of about -0.9 dB, however a 1.5 m long MWA applicator made from the same materials would have a total attenuation of almost -4.5 dB. This would cause the total power delivered to the antenna to drop from about 80% of the input power to 35% and cause significant heating of the applicator. However, despite the increased heating from cable attenuation, the temperature of a bronchoscopic applicator must remain below 50 °C along its entire length, exclusive of the active distal section, to avoid unintended thermal ablation along the length of the applicator and damage to the working channel of the bronchoscope. Second, it must be flexible, able to negotiate a tight bend radius (< 2”) if the bronchoscope must be fully articulated to reach the target site. MWA applicators in clinical use are rigid, needle-like designs

intended to be inserted in the target percutaneously. Finally, a bronchoscopic MWA applicator must have a very small outside diameter, less than 1.9 mm, to fit inside a bronchoscope's working channel. While the smallest possible MWA applicator diameter is desirable to minimize invasiveness, current percutaneous MWA applicators range from 17 gauge (1.47 mm OD) to 13 gauge (2.41 mm OD).

Assuming the principle use for a bronchoscopic MWA applicator would be the treatment of the growing number of small lung nodules (approximately 1cm in diameter) being identified by improved resolution chest CT, a target ablation zone diameter of 2 cm would provide the needed clinical margin of 5 mm in all directions for successful tumor treatment. Furthermore, a very spherical ablation zone is desired to contain thermal damage to the tumor while sparing as much healthy surrounding parenchyma as possible. Table 2-1 summarizes design constraints and goals.

Table 2-1 Design Constraints and Performance Goals

Parameter	Goal
Overall length	1.3 – 1.5 m
Outside diameter	< 1.9 mm
Ablation zone short axis	2 cm
Ablation zone axial ratio	≥ 0.7
On contact temperature	< 50° C

B. Bronchoscopic MWA Applicator Design

The proposed bronchoscopic MWA applicator consists of a monopole antenna at the distal end of a braided coaxial transmission line situated within the larger lumen of a dual lumen Grilamid™ extrusion. A monopole type antenna was selected based predominantly on its ease of fabrication, especially when utilizing a braided coaxial transmission cable. The monopole antenna was fabricated by stripping away a length of outer shield and dielectric material from the distal tip of the transmission cable equal to ¼ the effective wavelength of the incident electromagnetic wave in the surrounding medium. This effective wavelength takes into account the properties of the water, insulating catheter, and surrounding tissue [39]. Furthermore, a monopole antenna has a narrower diameter, is more flexible, and less fragile than other options such as a dipole or helix

allowing it to fit more conveniently inside the applicator and traverse a tight bend radius inside the bronchoscope's working channel. Other antenna types such as slot antenna were not investigated due to the impracticality of fabricating them with a braided coaxial transmission cable. The use of a balun/choke was precluded by the limited diameter of the device and the necessity to maintain maximum cooling water flow. A low-loss, 1.13 mm diameter, coaxial cable (D113LWS5BT, Wellshow, Keelung City, Taiwan) was selected based on its improved flexibility compared to semi-rigid options and comparable insertion loss (2.5 dB/m). A custom dual lumen outer catheter offered a larger internal cross-sectional area for circulating water flow and allowed operation at higher powers than uncooled or concentric tube designs.

Figure 2-1 shows the proposed longitudinal and transverse cross sections of the distal tip of the proposed bronchoscopic MWA applicator. A small length of the inner divider wall was removed at the distal end to facilitate a cooling water return path and the tip of the extrusion sealed with epoxy. The coaxial transmission line was inserted into the larger lumen of the catheter through a hemostasis valve (Qosina, Edgewood, NY) that also provided an inflow connection for the cooling water. The proximal tip of the smaller lumen was sealed with epoxy to prevent water inflow and an outflow opening was cut into the outer wall of the catheter on the smaller lumen side to allow for return flow through a Y-adapter (Qosina, Edgewood, NY).

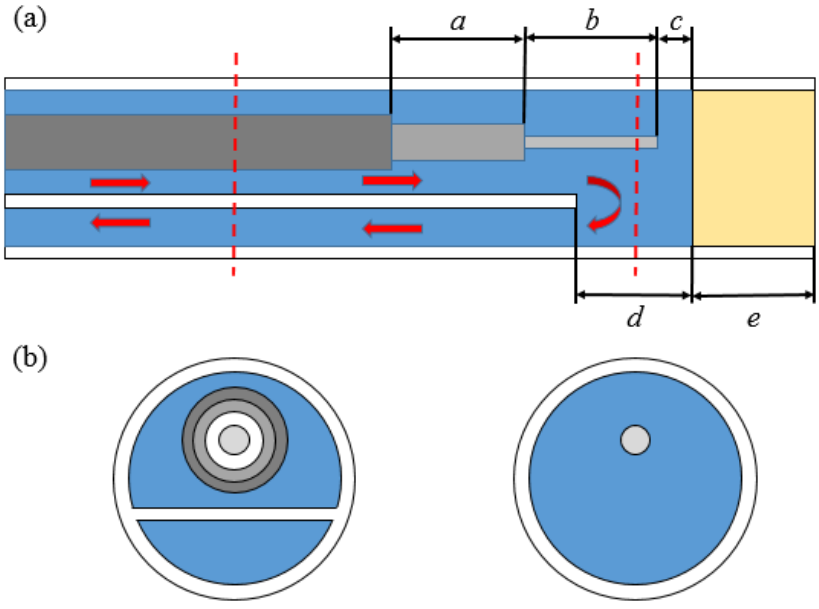

Figure 2-1 Section View of Bronchoscopic MWA Applicator

C. Finite Element Method Computational Model

A 3D finite element method (FEM) solver (COMSOL Multiphysics v5.3, COMSOL, INC. Burlington, MA) was used to model the electromagnetic radiation pattern and subsequent heat transfer from the bronchoscopic MWA applicator in a manner similar to that reported by McWilliams et al. and Sebek et al [40], [41]. The model was used to solve the Helmholtz electromagnetic wave equation:

$$\nabla^2\mathbf{E} - k_0^2\left(\varepsilon_r - \frac{j\sigma}{\omega\varepsilon_0}\right)\mathbf{E} = 0$$

where, E [V/m] is the electric field, k_0 [m^{-1}] is the free-space wavenumber, ε_r is relative permittivity, σ [S/m] is effective conductivity, ω [rad/s] is anugular frequency, and ε_0 [F/m] is permittivity of free-space. The distal tip of the antenna was modeled with a 6 cm insertion depth in an 8 cm diameter, 8 cm tall cylinder with the properties of muscle tissue. These dimensions provide a reasonable volume to assess the expected ablation volume while still being restrictive enough to limit computational time. Scattering boundary conditions were applied at the extents of the simulated liver domain. The material electromagnetic properties used in simulation are given in Table 2-2. The dual lumen catheter was assumed to be made from a material with similar electrical properties as polyimide.

For this initial design study, the surrounding tissue was modeled as liver tissue because it is a commonly used experimental model for evaluating ablation applicators designed for a range of different target tissue and tumor types and liver's electrical and thermal properties are well known [42]. Furthermore, the dielectric properties of lung tumors relative to the surrounding healthy lung are not well characterized and the temperature dependence of those properties is not known. It is unlikely that lung tumors participate in respiration, and therefore their electrical properties may be more similar to solid tissue, such as liver, compared to aerated lung. With a preliminary design validated through experimental use in liver, a follow-on study utilizing the same methodology may be used to revise a subsequent applicator design once more data on lung tumors and their electrical and thermal properties becomes available.

All coaxial cable conductors were modeled as perfect electrical conductors with infinite conductivity. A port boundary condition was established at the proximal of the coaxial cable dielectric and used to set the applicator's forward power. A non-uniform tetrahedral mesh was

constructed with maximum edge size of 0.01 mm at the port boundary, 0.14 mm throughout the applicator and 5 mm in the tissue domain. The maximum applicator mesh edge size was determined when further reducing the maximum element edge size did not change the resulting simulated S_{11} by more than 0.1 dB. With the above mesh settings, a static frequency domain solution took about nine minutes to compute with an Intel i5 processor and 32 GB of memory. Several applicator dimensions and materials were set specifically by the coaxial cable selection and optimized dual lumen catheter design. The remaining design variables (lengths a-e in Figure 2-1) were optimized through successive frequency domain parametric sweeps and selection of the length with the best impedance matching (most negative S_{11}). Based on tolerances expected for hand fabrication, the minimum variation for variable antenna dimensions was set at 1 mm.

Using a final applicator design optimized for electromagnetic performance, Pennes' bioheat equation was then used to compute the transient temperature profiles within the tissue:

$$\rho c(\mathbf{T})\frac{\partial \mathbf{T}}{\partial t} = \nabla \cdot k(T)\nabla \mathbf{T} + \mathbf{Q}_{mw} - \omega_{bl}(\mathbf{T} - \mathbf{T}_{bl})$$

where ρc is volumetric heat capacity [$Jm^{-3}K^{-1}$], T is temperature [K], k is thermal conductivity [$Wm^{-1}K^{-1}$], ω_{bl} is blood perfusion [$Wm^{-3}K^{-1}$], and T_{bl} is the temperature of blood. Table 2-2 lists the tissue biophysical properties used in simulation.

Table 2-2 Material Electrical/Thermal Properties

Parameter	Value	Unit	Temperature Dependency
Liver relative permittivity, ε_r [43]	43.0	-	Smoothed Step [44], [45]
Liver electric conductivity, σ [43]	1.69	S/m	Smoothed Step [44], [45]
Water relative permittivity, ε_r	77.6	-	Constant
Water electric conductivity, σ	1.31	S/m	Constant
FEP, ε_r [46]	2.1	-	Constant
Polyimide, ε_r [46]	3.4	-	Constant
Density, ρ [47]	1050	kgm^{-3}	Constant
Specific heat capacity, c [47]	3600	$Jkg^{-1}K^{-1}$	Piecewise Constant [47]
Thermal conductivity, k [47]	0.50	$Wm^{-1}K^{-1}$	Constant
Blood perfusion rate, ω_{bl} [47]	1400	$Wm^{-3}K^{-1}$	Smoothed Step [47]

The initial temperature of the tissue domain was set to 37 °C to mimic living tissue. To simulate the forced cooling of the applicator, a 38 °C fixed temperature boundary condition was applied on the outer surface of the catheter for 30 W simulations and 47 °C for 45 W simulations. These boundary conditions are an approximation to account for microwave heating of the chilled cooling water near the antenna, heat transfer from attenuation losses in the long transmission cable, and heat transfer from the surrounding tissue to the applicator surface. The specific temperature values were selected based on surface temperature measurements of fabricated applicators taken slightly proximal to the surface of the tissue sample during experimental ablations. The use of isothermal boundary conditions as an approximation to model forced cooling of the applicator has been previously proposed in literature [48]. Temperature dependence was implemented for tissue specific heat capacity to account for the latent heat of vaporization of the water in the tissue. Temperature dependence was also implemented for tissue relative permittivity and conductivity to account for changes as tissue is heated and desiccated [44], [49]. A piecewise linear approximation with a constant second-derivative that reduced relative permittivity and conductivity to 10% of initial values over a 70-degree transition zone centered on 80 °C was used. At a tissue temperature of 60 °C blood perfusion, ω_{bl}, was simulated to go to 0 simulating microvascular stasis for *in vivo* simulations (blood perfusion was not included for *ex vivo simulations).* An implicit transient solver was used with a maximum time step of 5 s where at each step temperature dependent thermal and electrical properties were updated. Input power levels of 13.84 W and 20.75 W were used in the computational models to account for the attenuation of the 1.3 m long transmission line (-3.36 dB) in prototype applicators operated at input powers of 30 and 45 W. An isothermal temperature contour at 55 °C was used to mark the extent of the simulated thermal ablation zone [3].

In addition to including the effects of blood perfusion, *in vivo* simulations also modeled a 1 cm diameter hypothetical tumor with tissue properties identical to liver surrounded by a lung tissue which oscillated between the electrical properties of inflated and deflated lung (inflated lung ε_r = 20.4, σ = 0.80; deflated lung ε_r = 48.4, σ = 1.68) to model the effects of breathing. The period of the oscillation was chosen to be 8 s, similar to the resting breathing rate in humans.

D. Experimental Evaluation

The applicator's thermal ablation zone profile was evaluated in *ex vivo* bovine liver. The applicator was inserted 6 cm into to 10 cm^3 samples that had been warmed to ~34 °C in a temperature-controlled water bath while sealed in water-tight plastic bags. A peristaltic pump (Cole-Parmer, Vernon Hills, IL) was used to circulate ice water through the applicator at a flow rate of approximately 20 mL/min. A series of four ablations were performed at 30 W and 45 W for 5 and 10 minutes each. MW power was supplied using a commercial microwave generator (Sairem, Neyron, France) and measured at the applicator SMA jack with a Bird 7022 power sensor (Bird Technologies, Solon, OH). Following ablation, tissue samples were sliced along the axis of the applicator to measure and document the length, width, and shape of the ablation zone based on the extent of tissue whitening.

III. Results

Table 2-3 lists the design parameters evaluated, the range of values tested, the minimum and maximum resulting S_{11}, the sensitivity of S_{11} to a change in the tested parameter (the range of S_{11} divided by the range of the parameter), and the optimized values. Figure 2-2 shows the antenna length (b) was by far the most sensitive parameter to variation with the length of FEP jacket stripped from the outer conductor (a) also having a moderate effect on overall impedance matching. The other parameters (c-e) did not appear to have a significant impact on the antenna's overall impedance matching and could therefore be further optimized based on thermal or manufacturing criteria. The distance the antenna is separated from the plug (c) is an important consideration since there may be some dimensional dislocation inside the device as the transmission cable and surrounding catheter take slightly different paths through the curves in a bronchoscope. Therefore, a minimum gap distance should be maintained between the antenna and plug to prevent damage to the fragile monopole antenna. Similarly, the plug length (e) is an important consideration to maintaining applicator durability when penetrating a tumor/tissue and for watertight integrity. The flow return path established by removing part of the catheter's dividing wall (d) could also have significant impacts on device cooling and circulating water flowrate.

Table 2-3 Parametric Optimization

Parameter	*a*	*b*	*c*	*d*	*e*
Range (mm)	1 - 8	3 - 16	1 – 5	1 - 8	1 – 5
Max s11 (dB)	-8.52	-3.45	-10.19	-10.31	-10.63
Min s11 (dB)	-10.67	-10.67	-10.67	-10.67	-10.67
Sensitivity	0.269	0.516	0.096	0.045	0.008
Optimized Value (mm)	6	7	1	5	2

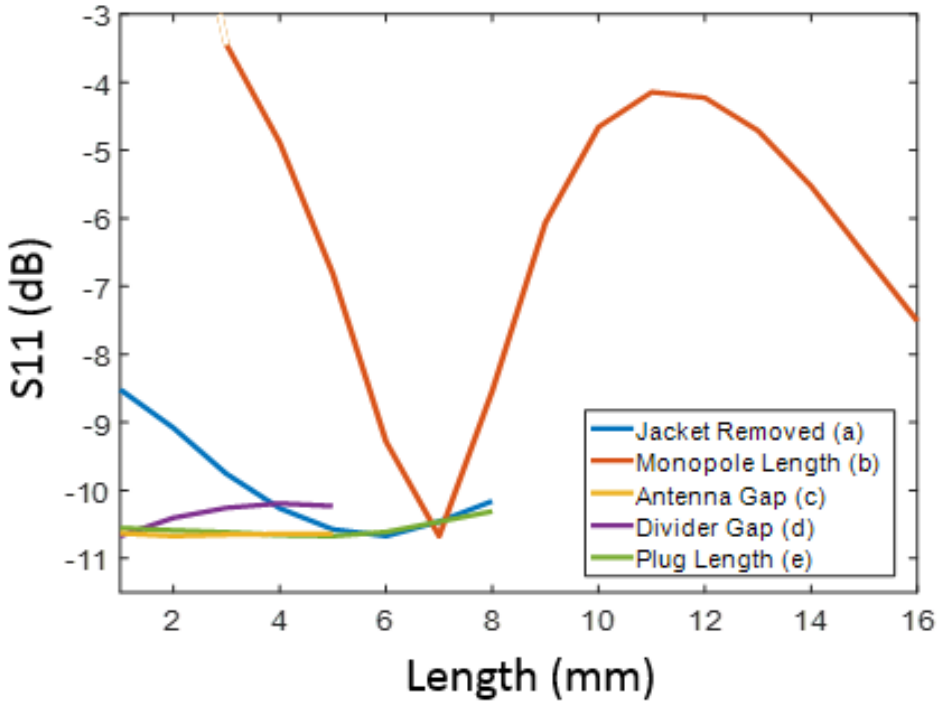

Figure 2-2 Effect of Varying Antenna Parameter on S11 (with all other parameters held constant at optimal value)

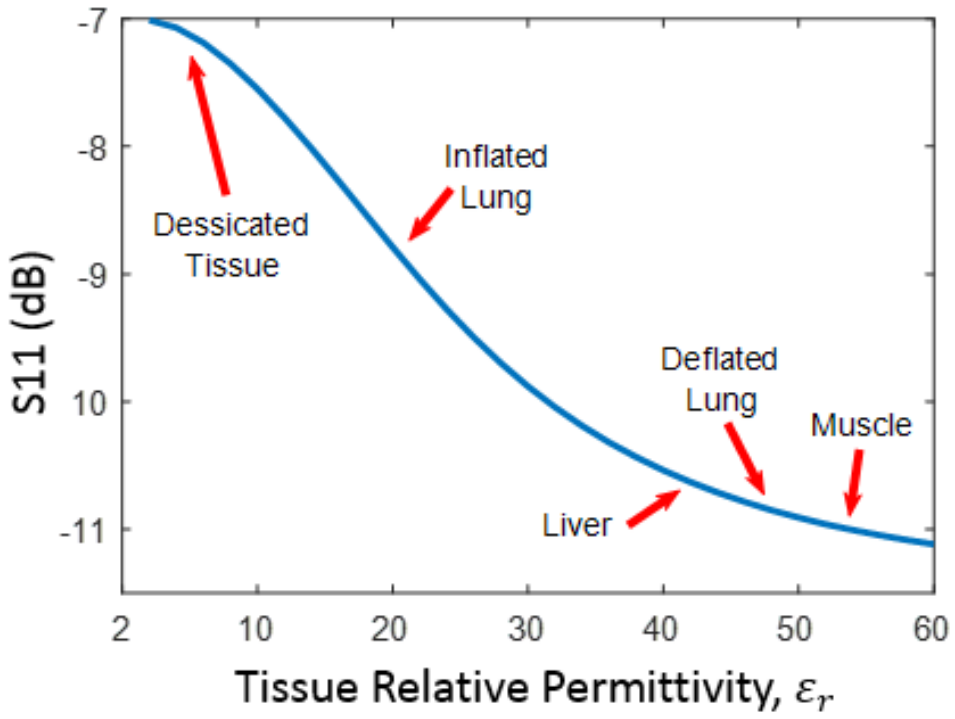

Figure 2-3 Applicator S11 as a Function of Tissue Permittivity

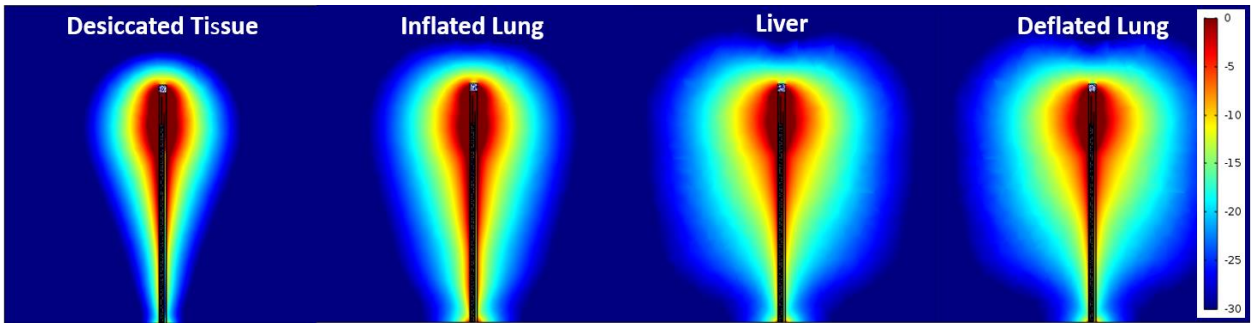

Figure 2-4 Bronchoscopic MWA Applicator Normalized SAR Profile for Various Tissues (dB scale, normalizing factor $10*\log_{10}(emw.Qe/10^7)$)

Considering a bronchoscopic MWA applicator would eventually be used in lung tumors with a potential broad range of specific tissue properties and solid to semi-solid tumor types, a sweep of possible tissue relative permittivities was also performed and the corresponding simulated values of antenna reflection coefficient are shown in Figure 2-3. Also, Figure 2-4 shows the applicator's normalized SAR pattern over various tissues. From these Figures, it can be seen that an applicator optimized for use in liver tissue could still be expected to perform reasonably well in a variety of other tissues; therefore, by extension, an applicator optimized for use in lung

using the techniques described in this study could be expected to perform reasonably well in a variety of tissue and tumor types.

1.3 m long prototype bronchoscopic MWA applicators were fabricated using the optimized dimensions (Figure 2-5). Figure 2-6 (top) (next page) gives the impedance matching of the applicator evaluated by measuring the broadband reflection coefficient using a HP 8753D vector network analyzer (VNA) (Keysight, Santa Rosa, CA) while inserted 6 cm into *ex vivo* bovine liver tissue (blue line).

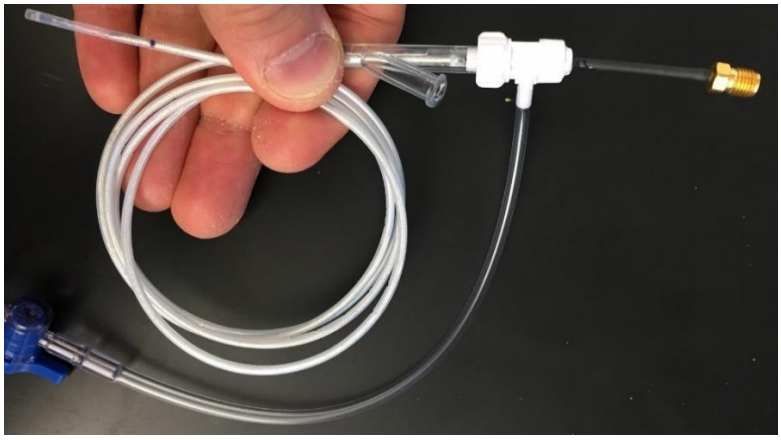

Figure 2-5 Fabricated Proof-of-Concept Bronchoscopic MWA Applicator

In the FEM implementation of the bronchoscopic MWA applicator, the coaxial cable feeding the antenna was modeled as a short (~6 cm) lossless transmission line. However, per the manufacturer datasheets, the 1.13 mm diameter coaxial cable used in the prototype applicators had an insertion loss of 2.5 dB/m at 2.4 GHz. The result of using this long transmission line is a significant amount of attenuation of not only the incident EM wave, but also the reflected wave. Therefore, the measured S_{11} of a fabricated bronchoscopic applicator would appear to be more negative than simulation results by approximately the value of the insertion loss of a transmission cable with twice the length of the applicator. (see Figure 2-6 top). Figure 2-6 (middle) shows the S_{21} of a 2.6 m female SMA to female SMA jumper cable measured with the VNA. At 2.45 GHz the total attenuation was 6.72 dB (or 2.58 dB/m). Figure 2-6 (bottom) shows when corrected for the un-modeled transmission line attenuation, the overall shape of the prototype's broadband reflection coefficient (blue line) matches the simulation results reasonably well (red line).

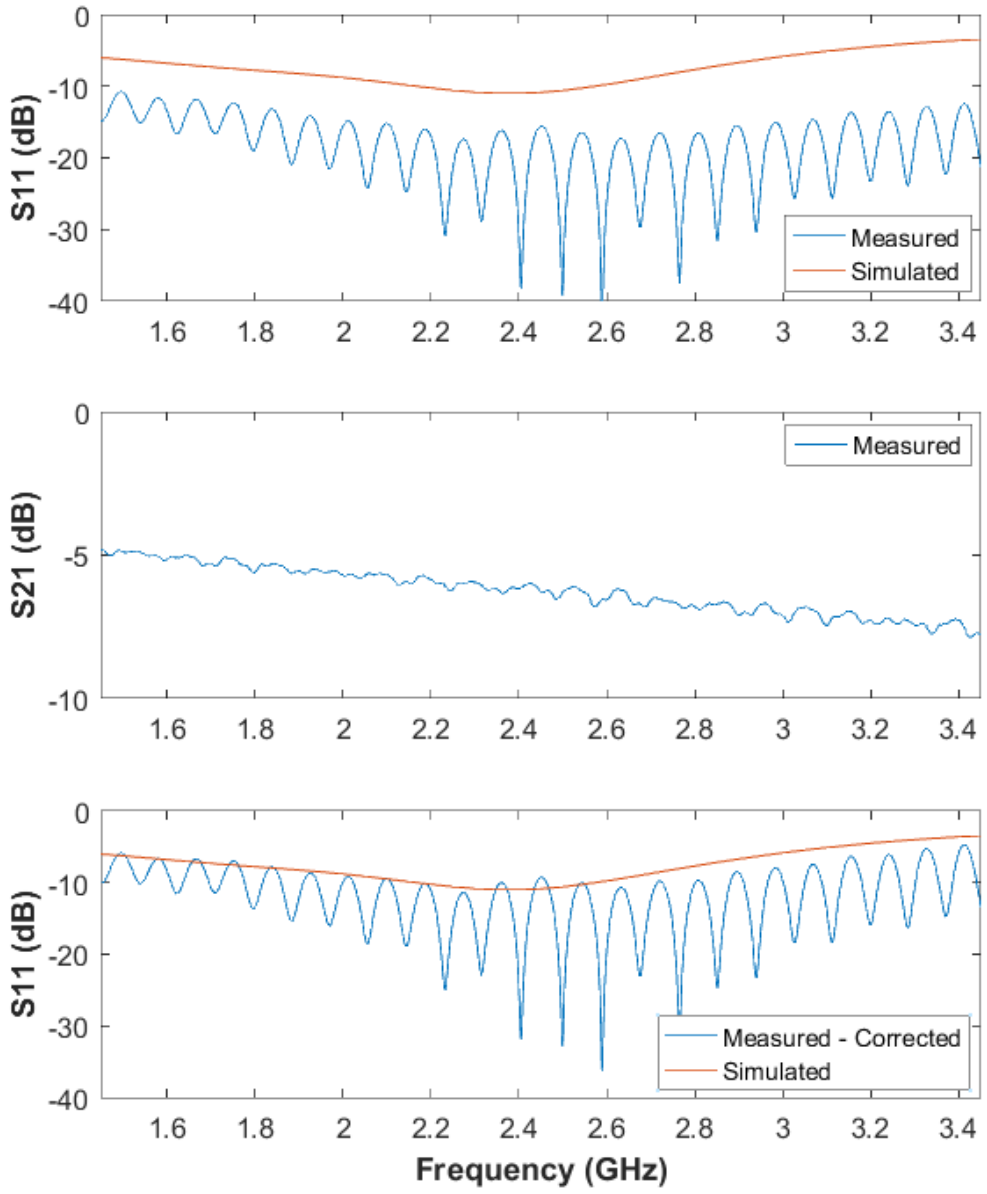

Figure 2-6 Measured and Simulated Impedance Matching (top), 2.6 m Transmission Cable Insertion Loss (middle), and Corrected Applicator Impedance Matching (bottom)

Figure 2-7 provides a visual comparison of experimental ablation zones to simulation. Table 2-4 provides a summary of experimental and simulated ablation zone width, height, and axial ratio.

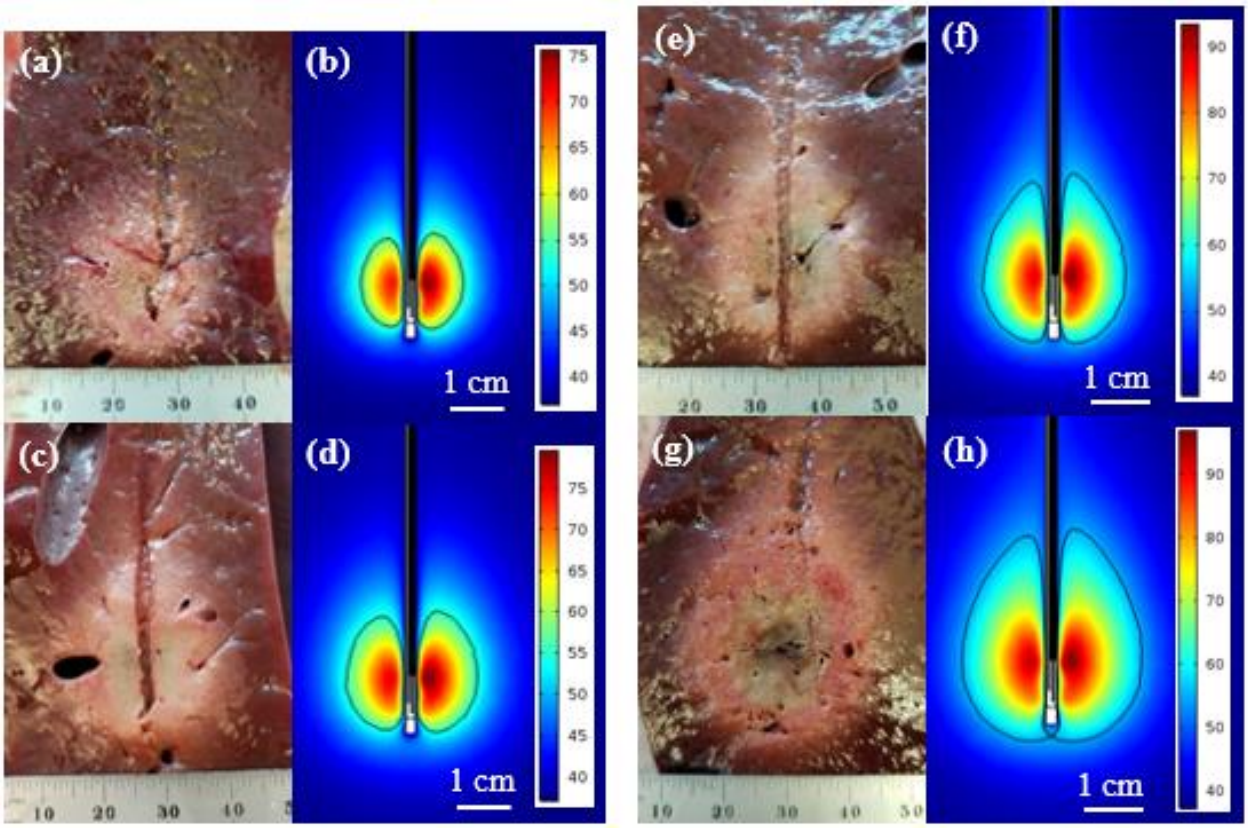

Figure 2-7 Experimental vs Simulated Ablation Zones for 30 W for 5 min (a-b), 30 W for 10 min (c-d), 45 W for 5 min (e-f), and 45 W for 10 min (g-h). Temperature scale is °C and black contour line is 55 °C.

Table 2-4 Experimental (Mean +/- STD) and Simulated Ablation Zone Results

Parameter	30 W 5 min	30 W 10 min	45 W 5 min	45 W 10 min
Width (mm)				
Measured	19.3 +/- 0.8	25.0 +/- 0.7	24.5 +/- 0.5	31.0 +/- 2.9
Simulated	19	25	24	31
Height (mm)				
Measured	22.3 +/- 1.3	32.3 +/- 0.8	33.5 +/- 1.5	42.25 +/- 1.9
Simulated	18	23	29	36
Axial Ratio				
Measured	0.87 +/- 0.03	0.78 +/- 0.05	0.73 +/- 0.04	0.73 +/- 0.05
Simulated	1.06	1.09	0.83	0.86

In vivo simulations conducted with a simplified 2D axisymmetric model at 45W for 10 minutes which included a 1 cm tumor, time-varying lung tissue electrical properties, and blood perfusion thermal losses gave a thermal ablation zone 2.3 cm wide by 4.0 cm long and an axial ratio of 0.58.

IV. Discussion

This study was undertaken to design a flexible MWA applicator suitable for thermal ablation of lung tumors via a bronchoscopic approach. The proposed design utilizes a long, flexible, braided coaxial transmission line with a monopole antenna housed in a custom dual lumen extrusion that provides a flow path for circulating cooling water. A simulation-based approach was employed to minimize the antenna reflection coefficient at 2.45 GHz and proof-of-concept applicators were fabricated and their ablation performance evaluated in *ex* vivo bovine liver as a first step in developing a model that could be used to optimize the applicator for use in lung tumor tissue. Since most MWA clinical and regulatory approval experience is based on initial work in liver tissue, with individual physicians later cross-applying their experience to treat other tissues, using the more well-documented tissue properties of liver could still be considered an acceptable starting point for device design. Experimental thermal ablation zones matched simulated widths very closely, however, simulations underestimated the experimental lengths by approximately 15-40%.

As shown in Figure 2-6, the slightly off-center positioning of the antenna inside the applicator due to the outer extrusion's dual lumen design did produce a slightly asymmetrical heating pattern. This can be attributed to the relatively longer radial length of water on the bottom of the device as shown in Figure 2-1. As the radiated electromagnetic waves travel through a greater distance of water, they are attenuated more than on the opposite side of the applicator. However, the effect on the symmetry of the overall ablation zone was negligible in both simulation and experiments.

Initial simulations indicated only two of the five optimized antenna dimensions had a significant effect on impedance matching, with antenna length being the most dominant as expected. This could potentially allow for the use of a simplified 2D axis-symmetric model for less computational intensive implementation of advanced coupled temperature and time dependent models. Furthermore, this reduction in potential critical dimensions allows for more freedom of

design for consideration of other factors such as cost, ease of manufacturing, and mechanical durability.

Although the optimized applicator utilized water cooling to remove waste heat from attenuation along the length of the applicator and reduce antenna dimensions due to its relatively high relative permittivity ($\varepsilon_r \approx 78$), its high conductivity ($\sigma \approx 1.3$ [S/m]) caused increased electromagnetic losses inside the applicator. This not only reduced the total energy available to heat the target tissue, but also raised the temperature of the cooling water, limiting the power the applicator could handle without exceeding on contact temperature limits. The use of other materials with a similar relative permittivity, such as titanium dioxide ($\varepsilon_r \approx 85$-100), that also have a much lower conductivity could potentially result in delivering a higher percentage of applied power to the target tissue. Applicators with these materials may also be able to operate at higher applied powers due to less internal heat generation affecting device cooling. Furthermore, combining low-loss ceramic dielectric materials near the distal tip of the antenna with more lossy materials near the base of the antenna could selectively attenuate the electromagnetic field to produce a more spherical radiation pattern.

While the proposed applicator was not exceptionally well matched at the desired operating frequency ($S_{11} \approx -10.7$ dB), the extent of the thermal ablation zones still met the minimum design criteria, including *in vivo* simulations which included a simple tumor model, time-varying lung tissue electrical properties, and thermal losses to blood perfusion. The applicator also had a good broadband response and could be expected to perform reasonably well across a range of potential tissue types. This is important because the physical and electric properties of lung tumors, especially at higher frequencies or elevated temperatures, are not well reported in the literature. Lung tumor properties are anticipated to be highly variable and dependent on the specific tumor's biology (i.e. primary cancer vs. metastatic disease) and physical characteristics (i.e. sold vs. semi-solid). Furthermore, even healthy lung has highly variable electrical properties with inflated lung having approximately half the relative permittivity and conductivity of deflated lung. Nevertheless, currently available percutaneous MWA applicators are being employed to treat lung tumors, which sets a theoretical precedent for MWA ablation in lung though other approaches [12], [23], [27]. As shown in Table 2-5, the proposed bronchoscopic MWA applicator has similar performance to currently available percutaneous MWA devices evaluated in *ex vivo* liver. Dimensions are given for ablations at 60 W for 5 minutes except for the Emprint device which is given for 100 W for 5

minutes. The bronchoscopic MWA applicator dimension are given for ablations at 45 W for 5 min, measured at the applicator connector (~60 W at the generator). Some discrepancies in actual applied power may be expected depending on if power is measured at the generator or at the applicator connection (due to attenuation in interconnecting cabling). More robust second-generation applicators operating at higher powers offer the potential to produce ablations nearly equivalent to percutaneous applicators.

Table 2-5 Comparison of MWA Applicators

System/Manufacturer	*Width (cm)*	*Length (cm)*	*Axial ratio*	*Gauge*
Certus – J&J/Neuwave	2.64	4.14	0.64	17
AveCure - Medwaves	3.00	5.00	0.60	14
Amica – HS S.p.A.	3.20	4.40	0.73	11
Solero - Angiodynamics	3.50	3.90	0.90	18
Emprint - Medtronic	4.00	4.20	1.00	13
Bronchoscopic MWA	2.45	3.35	0.73	~15

In addition to the absence of a simulated or experimental model of the ultimate target tissue, this study faced other limitations. Although used in literature, modeling the circulating water cooling effects as an isothermal boundary in simulations is a potentially significant oversimplification. Given some unique aspects of this applicator design, such as the long length of attenuation heat conduction, heat transfer though the thin lumen dividing wall, and electromagnetic absorption in the water near the antenna element, there could reasonably be expected to be a large temperature gradient along the length of applicator inserted in the target tissue. This thermal gradient could in turn have an appreciable effect on the simulated thermal ablation pattern. Given the general underestimation of simulated thermal ablation zone lengths given in Table 2-4, it is likely circulating water and applicator wall temperatures near the antenna are much higher than modeled. Accurately modeling the length of ablation zones and the temperatures achieved near the applicator are challenges which have been noted in the literature [50]. Developing a more accurate model of applicator wall temperatures, such as an exponential or piecewise linear gradient, is an area of possible future work.

Additional limitations involved the hand fabrication of the applicator. In all cases, fabricated dimensions were expected to be within a tolerance of 1 mm, however, this could have still had a significant impact on overall performance. Additionally, some materials and methods used in fabrication would need to be modified to meet biocompatibility standards, durability expectations, or other requirements for future clinical use.

V. Conclusion

In this study, simulation-based optimization techniques were utilized to design a bronchoscopic MWA applicator that needed to meet a range of practical performance goals. Proof-of-concept antennas were fabricated and experiments in *ex vivo* bovine liver were used to compare experimental impedance matching and thermal ablation zones to simulations. When calibrating for the effects of this applicator's long coaxial transmission cable, the broadband reflection coefficient of the prototype applicator matched well with simulated results. The overall sizes of the experimental thermal ablation zones were also in good comparison to simulated results with the exception that the experimental results had a more teardrop shape with the ablation zone extending further along the length of the applicator than simulated. This may be due to inaccurate modeling of effect of the circulating cooling water as an isothermal temperature boundary in simulations. Further analysis of the results indicated a 2D axisymmetric model simplification may be warranted for more computational resource intensive modeling applications and some possible antenna design parameters do not have a significant effect on electromagnetic performance and may be best optimized through other overall considerations. The modeling and optimization techniques described in this paper could be used to re-optimize this, or other similar devices, for use in other target tissues or for fabrication using other materials.

Chapter 3 - Future Work

Some of my future work will center on improving the applicator outer wall temperature model in my coupled electromagnetic heat transfer FEM simulations. Figure 2-7 highlights the inaccuracies of using an isothermal applicator wall temperature boundary conditions as the simulations do not show the same teardrop shape as the experiments and they also underestimate ablation length. It makes intuitive sense that the temperature along the applicator wall is not isothermal, but instead has some gradient that depends on applied power, cooling water flow, and time. One possible model might use an exponential gradient along the applicator wall which would help account for microwave heating of the cooling water near the antenna, heat transfer from attenuation in the coaxial cable to the cooling water, and heat transfer from the applicator wall itself to or from the surrounding tissue. Assuming the temperature at distal tip of the applicator would remain suppressed around 100 °C due to the latent heat of vaporization as water is slowly driven from tissue at moderately low input powers, the maximum extent of the visual ablation zone near the applicator wall represents 55 °C, and a third proximal surface applicator surface temperature could be measured with a thermocouple, three points could be used to extrapolate an exponential function for the boundary temperature of the MWA applicator. A piecewise linear approximation using a similar process may also add sufficient accuracy while minimizing computational resources.

Other future work will focus on improving the bronchoscopic MWA applicator by developing new designs that will reduce the power lost in cooling water surrounding the antenna, thereby increasing the power delivered to the target tissue and reducing the undesired heating of the applicator. This could allow higher power operation and the ablation of larger tumors. These advanced designs may incorporate low-loss ceramics or polymers to partially encapsulate the

antenna. Only partially encapsulating the antenna may have the effect of reducing EM loss near the tip of the device while selectively attenuating the field towards the shaft of the device to create a more spherical ablation zone with a more clinically desirable thermal ablation profile. This work will also need to include research into advanced medical device fabrication techniques to ensure the adequate manufacturing precision and quality to produce a reliable clinical device.

Additional work will include more detailed characterization of the electric properties of lung tissue, including a range of lung tumors. This characterization will need to include the effects of respiration in *in vivo* lung which causes the air content, and therefore, tissue electric properties to vary with time. These time varying changes in living lung tissue electric properties cause a time varying change in antenna reflected power during ablation. Combining the time varying nature of lung tissue with the effect of desiccation and cell death during ablation may provide a way to control and monitor ablation progress real-time as the amplitude in reflected power oscillations due to respiration ceases near the MWA applicator.

Other work will also be necessary to integrate bronchoscopic MWA applicators with the other components comprising the complete bronchoscopic MWA system. This may include sourcing a microwave signal generator and amplifier, cooling water pump, and interconnecting cabling and tubing. It will also require integration of the ablation energy delivery system with the Archimedes^{TM} treatment planning and guidance platform. This would include detailed characterization of the expected ablation zone in lung tissue, including in a range of tumor types, for use in planning treatment power and duration and applicator placement.

This integrated system would then need to be evaluated clinically to assess how the effects of air flow, blood flow, and tumor biology alter ablation zone size and shape compared to predictions and evaluated histologically to compare thermal damage to that of percutaneous

ablation. Additional highly detailed modeling, simulations, and *ex vivo* and *in vivo* studies will be needed to show technical feasibility, safety, and efficacy, both during the regulatory approval process and during clinical trials.

Finally, I have also worked to improve the design and performance of a directional percutaneous MWA applicator. Integrating directionality, achieved primarily through the use of a hemispherical reflector, into a bronchoscopic MWA applicator could further expand clinical use and functionality.

References

[1] P. Wust *et al.*, "Hyperthermia in combined treatment of cancer," *Lancet Oncol.*, vol. 3, no. 8, pp. 487–497, Aug. 2002.

[2] J. A. Pearce, "Comparative analysis of mathematical models of cell death and thermal damage processes," *Int. J. Hyperthermia*, vol. 29, no. 4, pp. 262–280, Jun. 2013.

[3] W. C. Dewey, "Arrhenius relationships from the molecule and cell to the clinic," *Int. J. Hyperthermia*, vol. 25, no. 1, pp. 3–20, Feb. 2009.

[4] Salgaonkar Vasant A. *et al.*, "Model-based feasibility assessment and evaluation of prostate hyperthermia with a commercial MR-guided endorectal HIFU ablation array," *Med. Phys.*, vol. 41, no. 3, p. 033301, Feb. 2014.

[5] C. J. Diederich, W. H. Nau, and P. R. Stauffer, "Ultrasound applicators for interstitial thermal coagulation," *IEEE Trans. Ultrason. Ferroelectr. Freq. Control*, vol. 46, no. 5, pp. 1218–1228, Sep. 1999.

[6] C. M. Pacella, G. Francica, D. Costanzo, and G. Giuseppe, "Laser Ablation for Small Hepatocellular Carcinoma," *Radiology Research and Practice*, 2011. [Online]. Available: https://www.hindawi.com/journals/rrp/2011/595627/. [Accessed: 01-Apr-2018].

[7] G. Shafirstein *et al.*, "Conductive interstitial thermal therapy (CITT) inhibits recurrence and metastasis in rabbit VX2 carcinoma model," *Int. J. Hyperthermia*, vol. 25, no. 6, pp. 446–454, Sep. 2009.

[8] S. N. Goldberg, "Radiofrequency tumor ablation: principles and techniques," *Eur J Ultrasound J Eur Fed Soc Ultrasound Med Biol*, vol. 13, no. 2, pp. 129–147, Jun. 2001.

[9] M. Atoui, S. Gunda, D. Lakkireddy, and S. Mahapatra, "Radiofrequency Ablation to Prevent Sudden Cardiac Death," *Methodist DeBakey Cardiovasc. J.*, vol. 11, no. 2, pp. 121–128, 2015.

[10] L. A. Mynderse, C. G. Roehrborn, A. W. Partin, G. M. Preminger, and E. P. Coté, "Results of a 5-Year Multicenter Trial of a New Generation Cooled High Energy Transurethral Microwave Thermal Therapy Catheter for Benign Prostatic Hyperplasia," *J. Urol.*, vol. 185, no. 5, pp. 1804–1810, May 2011.

[11] J. Wong, N. Bremer, P. D. Weyker, and C. A. J. Webb, "Ultrasound-Guided Genicular Nerve Thermal Radiofrequency Ablation for Chronic Knee Pain," *Case Rep. Anesthesiol.*, vol. 2016, 2016.

[12] L. Sidoff and D. Dupuy, "Clinical experiences with microwave thermal ablation of lung malignancies," *Int. J. Hyperthermia*, 2016.

[13] H. Luyen, F. Gao, S. C. Hagness, and N. Behdad, "Microwave Ablation at 10.0 GHz Achieves Comparable Ablation Zones to 1.9 GHz in Ex Vivo Bovine Liver," *IEEE Trans. Biomed. Eng.*, vol. 61, no. 6, pp. 1702–1710, Jun. 2014.

[14] S. Curto, M. Taj-Eldin, D. Fairchild, and P. Prakash, "Microwave ablation at 915 MHz vs 2.45 GHz: A theoretical and experimental investigation," *Med. Phys.*, vol. 42, no. 11, pp. 6152–6161, Nov. 2015.

[15] "Dielectric Properties of Body Tissues: HTML clients." [Online]. Available: http://niremf.ifac.cnr.it/tissprop/htmlclie/htmlclie.php. [Accessed: 01-Apr-2018].

[16] G. D. Dodd, M. S. Frank, M. Aribandi, S. Chopra, and K. N. Chintapalli, "Radiofrequency thermal ablation: computer analysis of the size of the thermal injury created by overlapping ablations," *AJR Am. J. Roentgenol.*, vol. 177, no. 4, pp. 777–782, Oct. 2001.

[17] "Analysis of microwave ablation antenna optimization techniques - Etoz - 2018 - International Journal of RF and Microwave Computer-Aided Engineering - Wiley Online Library." [Online]. Available: https://onlinelibrary-wiley-com.er.lib.k-state.edu/doi/full/10.1002/mmce.21224. [Accessed: 01-Apr-2018].

[18] H. Luyen, S. C. Hagness, and N. Behdad, "A Minimally Invasive Coax-Fed Microwave Ablation Antenna With a Tapered Balun," *IEEE Trans. Antennas Propag.*, vol. 65, no. 12, pp. 7280–7287, Dec. 2017.

[19] P. Prakash*, M. C. Converse, J. G. Webster, and D. M. Mahvi, "An Optimal Sliding Choke Antenna for Hepatic Microwave Ablation," *IEEE Trans. Biomed. Eng.*, vol. 56, no. 10, pp. 2470–2476, Oct. 2009.

[20] P. Bernardi, M. Cavagnaro, J. C. Lin, S. Pisa, and E. Piuzzi, "Distribution of SAR and temperature elevation induced in a phantom by a microwave cardiac ablation catheter," *IEEE Trans. Microw. Theory Tech.*, vol. 52, no. 8, pp. 1978–1986, Aug. 2004.

[21] L. Winter *et al.*, "Magnetic resonance thermometry: Methodology, pitfalls and practical solutions," *Int. J. Hyperth. Off. J. Eur. Soc. Hyperthermic Oncol. North Am. Hyperth. Group*, vol. 32, no. 1, pp. 63–75, 2016.

[22] C. L. Brace, "Radiofrequency and Microwave Ablation of the Liver, Lung, Kidney, and Bone: What Are the Differences?," *Curr. Probl. Diagn. Radiol.*, vol. 38, no. 3, pp. 135–143, May 2009.

[23] M. W. Little, D. Chung, P. Boardman, F. V. Gleeson, and E. M. Anderson, "Microwave Ablation of Pulmonary Malignancies Using a Novel High-energy Antenna System," *Cardiovasc. Intervent. Radiol.*, vol. 36, no. 2, pp. 460–465, Apr. 2013.

[24] G. Deshazer, D. Merck, M. Hagmann, D. E. Dupuy, and P. Prakash, "Physical modeling of microwave ablation zone clinical margin variance," *Med. Phys.*, vol. 43, no. 4, pp. 1764–1776, Apr. 2016.

[25] G. A. Carberry, E. Nocerino, M. M. Cristescu, A. R. Smolock, F. T. Lee, and C. L. Brace, "Microwave Ablation of the Lung in a Porcine Model: Vessel Diameter Predicts Pulmonary Artery Occlusion," *Cardiovasc. Intervent. Radiol.*, vol. 40, no. 10, pp. 1609–1616, Oct. 2017.

[26] G. A. Carberry *et al.*, "Pulmonary Microwave Ablation Near the Heart: Antenna Positioning Can Mitigate Cardiac Complications in a Porcine Model," *Radiology*, vol. 282, no. 3, pp. 892–902, Mar. 2017.

[27] F. J. Wolf, B. Aswad, T. Ng, and D. E. Dupuy, "Intraoperative Microwave Ablation of Pulmonary Malignancies with Tumor Permittivity Feedback Control: Ablation and Resection Study in 10 Consecutive Patients," *Radiology*, vol. 262, no. 1, pp. 353–360, Jan. 2012.

[28] K. F. Chu and D. E. Dupuy, "Thermal ablation of tumours: biological mechanisms and advances in therapy," *Nat. Rev. Cancer*, vol. 14, no. 3, pp. 199–208, Mar. 2014.

[29] "Key statistics for lung cancer." [Online]. Available: http://www.cancer.org/cancer/lungcancer-non-smallcell/detailedguide/non-small-cell-lung-cancer-key-statistics. [Accessed: 11-Oct-2016].

[30] R. Eberhardt, N. Kahn, and F. J. F. Herth, "'Heat and Destroy': Bronchoscopic-Guided Therapy of Peripheral Lung Lesions," *Respir. Basel*, vol. 79, no. 4, pp. 265–73, Feb. 2010.

[31] Asano Fumihiro, "Advanced bronchoscopy for the diagnosis of peripheral pulmonary lesions," *Respir. Investig.*, vol. 54, no. 4, pp. 224–229, Jul. 2016.

[32] D. H. Sterman *et al.*, "High Yield of Bronchoscopic Transparenchymal Nodule Access Real-Time Image-Guided Sampling in a Novel Model of Small Pulmonary Nodules in Canines," *Chest*, vol. 147, no. 3, pp. 700–707, Mar. 2015.

[33] G. A. Silvestri *et al.*, "Feasibility and Safety of Bronchoscopic Transparenchymal Nodule Access in Canines: A New Real-Time Image-Guided Approach to Lung Lesions," *Chest*, vol. 145, no. 4, pp. 833–838, Apr. 2014.

[34] D. Liu and C. L. Brace, "CT imaging during microwave ablation: Analysis of spatial and temporal tissue contraction," *Med. Phys.*, vol. 41, no. 11, p. n/a-n/a, Nov. 2014.

[35] "Broncus Medical, Inc. | Archimedes™ System." [Online]. Available: http://www.broncus.com/products/archimedes/. [Accessed: 01-Apr-2018]

[36] Herth, F.J.F., “Bronchoscopic transparenchymal nodule access (BTPNA): First in human trial of a novel procedure for sampling solitary pulmonary nodules,” *Thorax*, vol. 70, no. 4, pp. 326–332, 2015.

[37] Ziemlewicz, Timothy J., “Percutaneous Microwave Ablation of Hepatocellular Carcinoma with a Gas-Cooled System: Initial Clinical Results with 107 Tumors,” *J. Vasc. Interv. Radiol.*, vol. 26, no. 1, pp. 62–68, 2015.

[38] P.-C. Liang, H.-S. Lai, T. T.-F. Shih, C.-H. Wu, and K.-W. Huang, “The pilot experience upon surgical ablation of large liver tumor by microwave system with tissue permittivity feedback control mechanism,” *BMC Surg.*, vol. 14, p. 82, Oct. 2014.

[39] R. W. P. King, B. S. Trembly, and J. W. Strohbehn, “The Electromagnetic Field of an Insulated Antenna in a Conducting Or Dielectric Medium,” *IEEE Trans. Microw. Theory Tech.*, vol. 31, no. 7, pp. 574–583, Jul. 1983.

[40] B. T. McWilliams, E. E. Schnell, S. Curto, T. M. Fahrbach, and P. Prakash, “A Directional Interstitial Antenna for Microwave Tissue Ablation: Theoretical and Experimental Investigation,” *IEEE Trans. Biomed. Eng.*, vol. 62, no. 9, pp. 2144–2150, Sep. 2015.

[41] J. Sebek, S. Curto, R. Bortel, and P. Prakash, “Analysis of minimally invasive directional antennas for microwave tissue ablation,” *Int. J. Hyperth. Off. J. Eur. Soc. Hyperthermic Oncol. North Am. Hyperth. Group*, vol. 33, no. 1, pp. 51–60, Feb. 2017.

[42] C. Amabile *et al.*, “Microwave ablation of primary and secondary liver tumours: ex vivo, in vivo, and clinical characterisation,” *Int. J. Hyperth. Off. J. Eur. Soc. Hyperthermic Oncol. North Am. Hyperth. Group*, vol. 33, no. 1, pp. 34–42, 2017.

[43] S. Gabriel, R. W. Lau, and C. Gabriel, “The dielectric properties of biological tissues: III. Parametric models for the dielectric spectrum of tissues,” *Phys. Med. Biol.*, vol. 41, no. 11, p. 2271, 1996.

[44] V. Lopresto, R. Pinto, and M. Cavagnaro, “Experimental characterisation of the thermal lesion induced by microwave ablation,” *Int. J. Hyperthermia*, vol. 30, no. 2, pp. 110–118, Mar. 2014.

[45] Z. Ji and C. L. Brace, “Expanded modeling of temperature-dependent dielectric properties for microwave thermal ablation,” *Phys. Med. Biol.*, vol. 56, no. 16, p. 5249, 2011.

[46] C. A. Balanis, *Advanced Engineering Electromagnetics*. Hoboken, NJ, USA: Wiley, 1982.

[47] S. K. Hall, E. H. Ooi, and S. J. Payne, “Cell death, perfusion and electrical parameters are critical in models of hepatic radiofrequency ablation,” *Int. J. Hyperthermia*, vol. 31, no. 5, pp. 538–550, Aug. 2015.

[48] Deshazer Garron, Hagmann Mark, Merck Derek, Sebek Jan, Moore Kent B., and Prakash Punit, "Computational modeling of 915 MHz microwave ablation: Comparative assessment of temperature-dependent tissue dielectric models," *Med. Phys.*, vol. 44, no. 9, pp. 4859–4868, May 2017.

[49] C. L. Brace, "Temperature-dependent dielectric properties of liver tissue measured during thermal ablation: Toward an improved numerical model," in *2008 30th Annual International Conference of the IEEE Engineering in Medicine and Biology Society*, 2008, pp. 230–233.

[50] M. Cavagnaro, R. Pinto, and V. Lopresto, "Numerical models to evaluate the temperature increase induced by ex vivo microwave thermal ablation," *Phys. Med. Biol.*, vol. 60, no. 8, p. 3287, 2015.